# Self-Assembly of a Catalytically Active Lipopeptide and Its Incorporation into Cubosomes

Valeria Castelletto,[†] Charlotte J. C. Edwards-Gayle,[†] Ian W. Hamley,*[,†] Juliane N. B. D. Pelin,[‡] Wendel A. Alves,[‡] Andrea M. Aguilar,[§] Jani Seitsonen,[∥] and Janne Ruokolainen[∥]

[†]Department of Chemistry, University of Reading, Reading RG6 6AD, United Kingdom

[‡]Centro de Ciências Naturais e Humanas, Federal do ABC, Santo André 09210-580, Brazil

[§]Instituto de Ciências Ambientais, Químicas e Farmacêuticas, Universidade Federal de São Paulo, Diadema 09972-270, Brazil

[∥]Nanomicroscopy Center, Aalto University, Puumiehenkuja 2, Espoo FIN-02150, Finland

Ⓢ *Supporting Information*
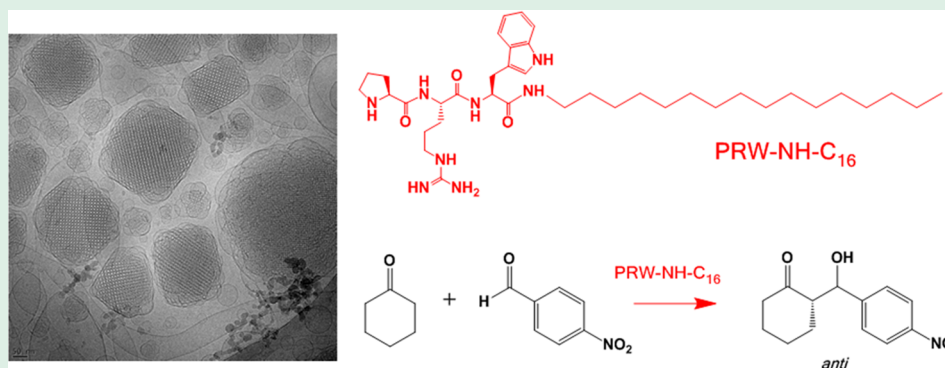
**ABSTRACT:** The self-assembly and biocatalytic activity of the proline-functionalized lipopeptide PRW-NH-C$_{16}$ are examined and compared to that of the related PRW−O-C$_{16}$ lipopeptide, which differs in having an ester linker between the lipid chain and tripeptide headgroup instead of an amide linker. Lipopeptide PRW-NH-C$_{16}$ self-assembles into spherical micelles above a critical aggregation concentration, similar to the behavior of PRW−O-C$_{16}$ reported previously [B. M. Soares et al. *Phys. Chem. Chem. Phys.*, 2017, 19, 1181—1189]. However, PRW-NH-C$_{16}$ shows an improved catalytic activity in a model aldol reaction. In addition, we explore the incorporation of the biocatalytic lipopeptide into lipid cubosomes. SAXS shows that increasing lipopeptide concentration leads to an expansion of the monoolein cubosome lattice spacing and a loss of long-range cubic order as the lipopeptide is encapsulated in the cubosomes. At higher loadings of lipopeptide, reduced cubosome formation is observed at the expense of vesicle formation. Our results show that the peptide−lipid chain linker does not influence self-assembly but does impart an improved biocatalytic activity. Furthermore, we show that lipopeptides can be incorporated into lipid cubosomes, leading to restructuring into vesicles at high loadings. These findings point the way toward the future development of bioactive lipopeptide assemblies and slow release cubosome-based delivery systems.

**KEYWORDS:** *lipopeptides, peptide amphiphiles, self-assembly, micelles, cubosomes, catalysis, aldol reaction*

## INTRODUCTION

Lipopeptides are versatile molecules, in which peptides are attached to lipid chains. This can lead to aqueous self-assembly of the amphiphilic molecules when lipopeptides bear hydrophilic peptide "headgroups". Various self-assembled structures including nanofibers, nanotapes, and micelles, have been reported.[1−6] In the self-assembled lipopeptide nanostructure, the peptide group is presented at the surface at high density, often leading to enhanced activity compared to the unlipidated (and unassembled) peptide.

Proline is an important residue in peptides with catalytic properties.[7−9] Miravet, Escuder, and co-workers have studied a series of proline peptide gelators, which are efficient catalysts of the nitro-aldol reaction, among others.[10−12] Lipopeptides

simply comprising alkylated proline have been shown to be efficient catalysts of direct aldol reactions in water and organic solvents, exhibiting high yields and excellent enantioselectivities,[13] in oil-in-water emulsions.[14] In a recent study, a lipopeptide PRW−O-C$_{16}$ bearing an N-terminal proline residue was designed to facilitate biocatalysis via a model aldol reaction. The peptide incorporates a charged arginine residue to improve solubility and a tryptophan residue for fluorescence detection.[8] This lipopeptide was shown to self-assemble into micelles above a critical aggregation concen-

tration, detected through intrinsic tryptophan fluorescence or using an added fluorophore probe (pyrene, the fluorescence of which is sensitive to the hydrophobic environment).[8] Because the ester bond in PRW−O-C$_{16}$ is susceptible to degradation (base or enzymatic hydrolysis), in the present work, we investigate the original peptide in comparison with an analogue with a peptide (amide) bond, which is expected to have an enhanced stability. In addition, we explore the incorporation of the lipopeptide into cubosomes with the intention of producing high surface area peptide-functionalized nanoparticles. The micellar environment is expected to enhance the catalytic reaction due to the high density presentation of proline residues at the surface, where there can also be local compartmentalization of the reagents.

Cubosomes are stable nanoscale aggregates of lipids forming bicontinuous cubic phases. They have attracted considerable attention due to potential application as nanomedicines able to entrap and subsequently slowly release encapsulated cargo due to diffusion out of the channels in the bicontinuous cubic structure.[15−18] The particles are typically stabilized by incorporation of small quantities of poly(ethylene oxide) [PEO]-containing block copolymers such as the Pluronic PEO−PPO-PEO [PPO: poly(propylene oxide)] poloxamer triblock copolymers.[19,20] The PEO chains form a steric stabilization barrier around the cubosome nanoparticles.

In the present work, we investigate incorporation of the lipopeptide PRW-NH-C$_{16}$ into cubosomes formed by monoolein (also known as glyceryl monooleate), which is a model system for lipid bicontinuous cubic phase formation, forming $Im\bar{3}m$ (primitive P or $Q^{229}$ or "plumbers nightmare" structure) and $Pn\bar{3}m$ ("double diamond" or D or $Q^{224}$ structure) cubic phases, depending on the concentration in water and the presence of poloxamers.[21−24] Monoolein is also widely used as the lipid component in cubosomes.[16,21,25] We formulate the cubosomes with the Pluronic F127, often used as a cubosome stabilizer.[16,20,21,25] There are only a few prior studies on peptide incorporation into cubosomes. The loading of cubosomes with antimicrobial peptides gramicidin A, alamethicin, and mellitin was investigated via small-angle X-ray scattering (SAXS), with up to 10 mol % incorporated before disruption of the cubic lattice structure.[26] In other studies, slow release of three other antimicrobial peptides from cubosomes was confirmed, and the antimicrobial activity was retained or even enhanced (depending on the antimicrobial peptide and the bacterium type), while antimicrobial peptide LL37, which is susceptible to degradation, was stabilized within cubosomes against proteolysis.[27,28] SAXS was used to investigate the retention of cubic structure within the lipid nanoparticles, and the effect of peptide loading on this was found to depend on peptide polarity.[27] To our knowledge, incorporation of lipopeptides into cubosomes has not previously been investigated, although we hypothesized that this would be a promising approach to load cubosomes with functionalized peptides due to the potential ability of the lipopeptide chains to insert into lipid membranes. Here, in addition to comparing the self-assembly and aldol catalysis activity of PRW-NH-C$_{16}$ and PRW−O-C$_{16}$ (shown in Scheme 1), we also use SAXS to probe incorporation of the ester-linkage free lipopeptide PRW-NH-C$_{16}$ into cubosomes formed by monoolein in the presence of Pluronic F127. With relevance to potential future applications of PRW-NH-C$_{16}$ as a biologically active molecule, we also examined its cytotoxicity against model fibroblast and

**Scheme 1. Molecular Structures of PRW-NH-C$_{16}$ and PRW−O-C$_{16}$**
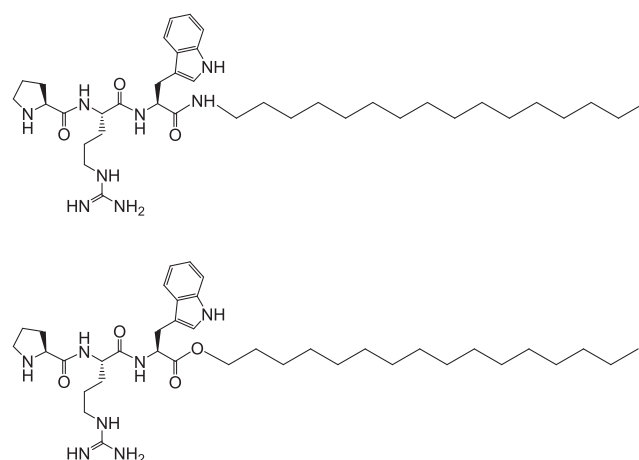


breast cancer cell lines. The cytotoxicity of PRW−O-C$_{16}$ has been reported previously.[29]

## ■ EXPERIMENTAL SECTION

**Materials.** Lipopeptide PRW-NH-C$_{16}$ (Scheme 1) was prepared by Peptide Synthetics (Peptide Protein Research), Farnham, U.K., with purity 99.6% confirmed by HPLC (XB-C18 Kinetex column, acetonitrile 50%−100% gradient). The molecular mass of PRW-NH-C$_{16}$ by ESI-MS is 680.96 g mol$^{-1}$ (680.98 g mol$^{-1}$ expected).

**Cubosome Preparation.** Cubosomes were prepared with 10 wt % monoolein (Mo) and 1 wt % Pluronic F127. Mo was obtained from Sigma-Aldrich (U.K.) while F127 was from a gift from BASF. To prepare the cubosomes, Mo was melted at 60 °C for 10 min inside an Eppendorf. After melting, enough 1 wt % F127 solution in water was added to the Eppendorf, in order to have 10 wt % Mo in the 1 wt % F127 solution. For cubosomes loaded with PRW-NH-C$_{16}$, the peptide powder was added to the melted Mo, and the sample was centrifuged at 30 000 rpm for 5 min, before the F127 solution was added. The concentration of lipopeptide was calculated with respect to the weight of 1 wt % F127 solution. The solution in the Eppendorf was sonicated with a high intensity ultrasonic probe, using 2 cycles at 30% amplitude of the maximum power, and 20 s pulses interrupted by 20 s breaks.

**Fluorescence Assays.** The intrinsic fluorescence of the tryptophan (Trp) side chain, together with a 8-anilino-1-naphthalenesulfonic acid (ANS) assay, were used to locate the critical aggregation concentration (cac). Spectra were recorded with a Varian Cary Eclipse fluorescence spectrometer with samples in 4 mm inner width quartz cuvettes. The ANS fluorophore is a probe sensitive to the hydrophobicity of its surrounding environment,[30] making it suitable to determine the cac. ANS assays were performed measuring spectra from 400 to 670 nm ($\lambda_{ex}$ = 356 nm), using a $2 \times 10^{-3}$ wt % ANS solution to solubilize the peptide. Trp emission fluorescence was measured from 350 to 550 nm, using aqueous PRW-NH-C$_{16}$ solutions, irradiated at $\lambda_{ex}$ = 280 nm.

**Release of PRW-NH-C$_{16}$ Loaded into Cubosomes.** Release of lipopeptide was monitored through dialysis. Samples containing 10 wt % Mo cubosomes were loaded with 0.1, 0.2, or 0.3 wt % PRW-NH-C$_{16}$. Aliquots of 20 $\mu$L of the solutions containing the lipopeptide-loaded Mo cubosomes were diluted using 180 $\mu$L of water and injected inside a Slide-A-Lyzer dialysis cassette (10 000 MWCO, 0.1−0.5 mL capacity; Thermo Fisher Scientific). Samples were allowed to dialyze in 60 mL of PBS (Dubelcco, Sigma-Aldrich. The PRW-NH-C$_{16}$ release was quantified by a fluorescamine (FLC) assay, since primary and secondary amines react with FLC to produce chromophores ($\lambda_{ex}$ = 380 nm, $\lambda_{em}$ ∼ 485 nm). For the FLC assay, 350 $\mu$L of sample was withdrawn after 24 h dialysis from the receptor side and mixed with 150 $\mu$L of 0.01 wt % FLC in acetone, just prior to the fluorescent intensity measurement (excitation at $\lambda$= 380 nm). The
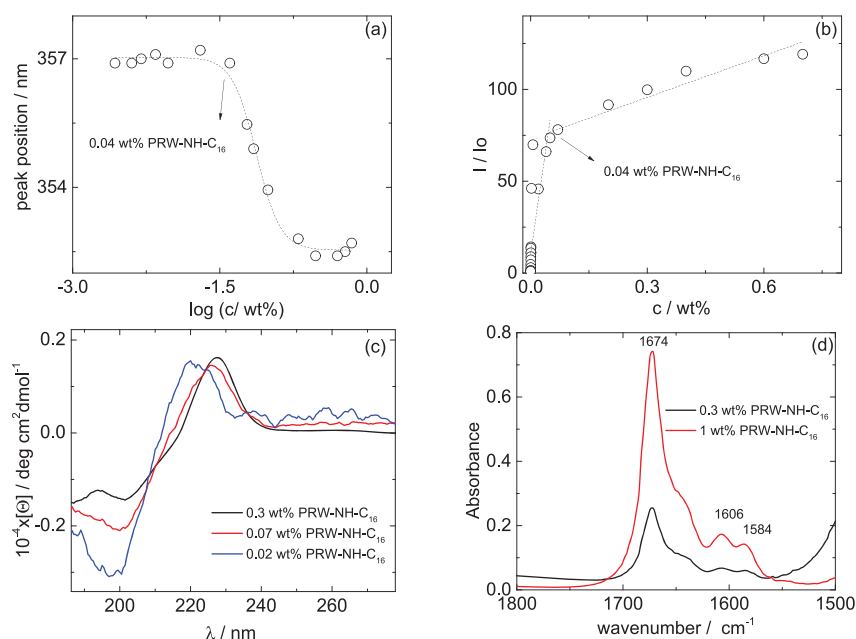
**Figure 1.** Spectroscopic characterization of PRW-NH-C$_{16}$ self-assembly in water: cac = 0.04 wt % PRW-NH-C$_{16}$ is determined from the concentration dependence of the emission wavelength of tryptophan (a) and the ANS assay (b); (c) CD spectra below and above the cac, (d) FTIR data above the cac.

FLC assay was performed using the same cell and instrument described above for the ANS assay.

**Circular Dichroism (CD) Spectroscopy.** CD spectra were recorded using a Chirascan spectropolarimeter (Applied Photophysics, U.K.). Solutions were placed in a quartz coverslip cuvette (0.01 mm thick). Spectra are presented with absorbance $A < 2$ at any measured point with a 0.5 nm step, 1 nm bandwidth, and 1 s collection time per step. The CD signal from the water background was subtracted from the CD data of the sample solutions.

**Fourier Transform Infrared (FTIR) Spectroscopy.** Spectra were recorded using a Nexus-FTIR spectrometer equipped with a DTGS detector. Samples were measured using a PEARL liquid cell. Spectra were scanned 128 times over the range of 900−4000 cm$^{-1}$.

**Cryogenic Transmission Electron Microscopy (Cryo-TEM).** Imaging was carried out using a field emission cryo-electron microscope (JEOL JEM-3200FSC), operating at 200 kV. Images were taken in bright field mode and using zero loss energy filtering (omega type) with a slit width of 20 eV. Micrographs were recorded using a Gatan Ultrascan 4000 CCD camera. The specimen temperature was maintained at −187 °C during the imaging. Vitrified specimens were prepared using an automated FEI Vitrobot device using Quantifoil 3.5/1 holey carbon copper grids with a hole size of 3.5 $\mu$m. Just prior to use, grids were plasma cleaned using a Gatan Solarus 9500 plasma cleaner and then transferred into the environmental chamber of a FEI Vitrobot at room temperature and 100% humidity. Thereafter, 3 $\mu$L of the sample solution was applied on the grid and it was blotted twice for 5 s and then vitrified in a 1:1 mixture of liquid ethane and propane at a temperature of −180 °C. The grids with vitrified sample solution were maintained at liquid nitrogen temperature and then cryo-transferred to the microscope.

**Small-Angle X-ray Scattering (SAXS).** SAXS experiments on solutions were performed using a BioSAXS robot on beamline BM29 (ESRF, Grenoble France) or on beamline B21 (Diamond, Didcot, U.K.). On ESRF beamline BM29, solutions were loaded into the 96-well plate of an EMBL BioSAXS robot and then injected via an automated sample exchanger into a quartz capillary (1.8 mm internal diameter) in the X-ray beam. The quartz capillary was enclosed in a vacuum chamber, in order to avoid air scattering. After the sample was injected in the capillary and reached the X-ray beam, the flow was stopped during the SAXS data acquisition. BM29 operated with an X-ray wavelength $\lambda = 1.03$ Å (12 keV). The images were captured using

a PILATUS 1 M detector, while data processing was performed using dedicated beamline software ISPYB. On Diamond beamline B21, solutions were loaded into the 96-well plate of an EMBL BioSAXS robot and then injected via an automated sample exchanger into a quartz capillary (1.8 mm internal diameter) in the X-ray beam. The quartz capillary was enclosed in a vacuum chamber, in order to avoid parasitic scattering. After the sample was injected in the capillary and reached the X-ray beam, the flow was stopped during the SAXS data acquisition. B21 operated with a fixed camera length (3.9 m) and fixed energy (12.4 keV). The images were captured using a PILATUS 2 M detector. Data processing was performed using dedicated beamline software ScÅtter.

**Catalytic Aldol Reaction.** The reaction of 109 $\mu$L of cyclohexanone (1.1 mmol), 3.0 mg of catalyst (4.4 $\mu$mol), and 13.2 mg of p-nitrobenzaldehyde (93.2 $\mu$mol), varying the amount of water (218 $\mu$L, 114 $\mu$L, no water) was monitored. The solutions were stirred at room temperature for 2 days. Then the mixtures were extracted with ethyl acetate four times, via centrifugation at 9000 rpm for 3 min. For the sample with no water, 0.5 mL of water was added to help in the extraction step to assist phase separation. The product was monitored by TLC chromatography, using a mixture 1:4 of ethyl acetate/hexane as an eluent and vanillin as a developer. After, the samples were kept on a desiccator under a high vacuum until totally dry, and then NMR measurements using a ($^1$H) Bruker Ultrashield 300 instrument were performed at 300 MHz, using deuterated chloroform as a solvent. The yield and diastereomer *anti/syn* ratio were calculated using the NMR spectrum obtained, for which the tetramethylsilane (TMS) was used as a reference.

**Cell Viability Assays.** In vitro cell culture was conducted using MCF-7 (ECACC 86012803), human breast cancer cells, or 161Br cells (ECACC 90011810), a human skin fibroblast cell line. 161Br cells were cultured in MEME (minimum essential medium Eagle's), with 2 mM glutamine, enriched with 15% fetal bovine serum (FBS), 1% nonessential amino acids (NEAA), and 1% antimicrobial/antifungal. MCF-7 was cultured with RPMI supplemented with 5% FBS and 1% antimicrobial/antifungal. All cells were maintained in a humidified atmosphere at 37 °C and 5% CO$_2$.

The viability effects of PRW-NH$_2$-C$_{16}$ was examined using an MTT (3-(4,5-dimethylthiazol-2-yl)-2,5-diphenyltetrazolium bromide) assay. Cells were seeded into a 96-well plate at $4 \times 10^4$ cells/mL and allowed to adhere for 24 h in 100 $\mu$L complete medium. After this, peptides

were dissolved in complete medium, and 100 $\mu$L of either medium and/or peptide solution was added, to give either control solution (complete medium only) or peptide solutions with concentrations in the range 0.005−0.1 wt %.

Cells were incubated for either 19 or 67 h. Following this, 20 $\mu$L MTT (5 mg/mL, in PBS) was pipetted into each well plate and allowed to incubate for 5 h (corresponding to a total 24 or 72 h treatment time, respectively). After this, the solution was removed from the wells and replaced with 100 $\mu$L DMSO per well, in order to dissolve the formazan crystals. Plates were incubated for 30 min and then analyzed using a UV microplate reader ($\lambda$ = 570 nm). Results are reported as a % cell viability compared to control (untreated) values.

## ■ RESULTS

**Self-Assembly of PRW-NH-C$_{16}$ Compared to PRW−O-C$_{16}$.** We first measured the critical aggregation concentration of PRW-NH-C$_{16}$ via two independent fluorescence probe methods. Figure 1a shows the concentration dependence of the intrinsic tryptophan fluorescence peak position (the original spectra are presented in Figure S1). The onset of the decrease in peak position indicates the critical aggregation concentration (cac). Above the cac, the tryptophan fluorescence peak wavelength decreases due to quenching reduction of the solvent relaxation effect due to the formation of self-assembled structures, within which this residue is less exposed to the aqueous environment.[31] The cac is determined to be (0.04 ± 0.01) wt %. This cac also corresponds to a maximum in fluorescence intensity (Figure S1b) as previously observed for PRW−O-C$_{16}$.[8] The same cac is determined from independent measurements using the ANS external fluorescence probe, as shown by the discontinuity in the fluorescence intensity shown in Figure 1b (the original fluorescence spectra are contained in Figure S2). The cac measured here for PRW-NH-C$_{16}$ is the same (within uncertainty) as the value 0.03 wt % (=0.44 mM) for PRW−O-C$_{16}$ reported previously.[8]

The CD spectra in Figure 1c suggest that PRW-NH-C$_{16}$ adopts a polyproline II (PPII) conformation above and below the cac,[32−34] although there is a shift in position of the positive maximum from 221 to 226 nm and a change in intensity of the negative minimum at 198−200 nm. These changes may be caused by a difference in the fractional content of peptide with unordered conformation (disordered conformations are typically characterized by broad minima near 200 nm and no maxima[32]). However, we note that quantitative interpretation of the CD spectra is complicated by the additional contribution from electronic transitions of the indole unit in the tryptophan residue. The amide I' FTIR spectra in Figure 1d confirm the PPII conformation. A broad band in the 1640−1645 cm$^{-1}$ range can be assigned to PPII, although it is difficult to distinguish this from random coil conformation based on FTIR.[32,35] The spectra are dominated by the peak at 1674 cm$^{-1}$ due to TFA counterions bound to the arginine residue.[36−38] The presence of this residue also gives rise to the peaks at 1606 and 1584 cm$^{-1}$ from arginine side chain stretching bands.[39,40] Peaks due to CH$_2$ stretching modes of the hexadecyl chains are observed at 2853 and 2926 cm$^{-1}$ (Figure S3).[41,42]

Having established that PRW-NH-C$_{16}$ undergoes aggregation into a structure in which the peptide retains a PPII conformation, we used a combination of direct electron microscopic imaging (cryo-TEM) and small-angle X-ray scattering (SAXS) to provide detailed information on the self-assembled nanostructure. Figure 2 shows a representative cryo-TEM image for a 1 wt % lipopeptide solution and the
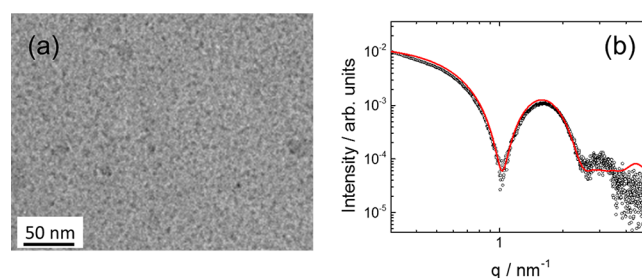


**Figure 2.** Self-assembly of PRW-NH-C$_{16}$. (a) Cryo-TEM image showing micelles. (b) SAXS data (open symbols) with a model fit (red line) to the core−shell micelle form factor.

SAXS intensity profile for a lipopeptide solution with a fitted core−shell micelle form factor. The cryo-TEM image shows the presence of spherical micelle structures with a diameter of (7 ± 2) nm. This is consistent with the model fit of the SAXS form factor, which yields an outer radius $R_1$ = (3.41 ± 0.03) nm and an inner core radius $R_2$ = 1.42 nm. The other fitted parameters (obtained using the core−shell spherical model I of SASfit software)[43] were the relative (electron density) contrast $\eta$ = 9.2 × 10$^{-4}$ and the relative core−shell electron density ratio $\mu$ = −2.47. A flat background BG = 0.6 was also included in the model. The model indicates a dense core region comprising the lipid chains surrounded by the less dense tripeptide corona. Clusters of micelles were noted in some regions of the TEM grid (as shown for example in Figure S4). The finding that PRW-NH-C$_{16}$ forms spherical micelles is consistent with the previous results for PRW−O-C$_{16}$, which forms slightly smaller micelles with a radius of 3.1 nm.[8]

**Catalytic Activity of PRW-NH-C16 in Aldol Reaction.** To facilitate comparisons, we used the same model aldol reaction to test the catalytic activity of PRW-NH-C$_{16}$ as previously used in tests with PRW−O-C$_{16}$.[8] The reaction scheme and results (yield and *anti/syn* stereoselectivity) are shown in Table 1. Using 5 mol % of PRW-NH-C$_{16}$ lipopeptide as a catalyst, the influence on the conversion factor and diastereoselectivity of products was observed. Two parameters were adjusted to influence the catalytic process: the use of HFIP (hexafluoro-2-propanol) to dissolve the lipopeptide before starting the aldol reactions and the water content in the systems. Considering entries 1 and 2 in Table 1, corresponding to the presence and absence, respectively, of HFIP, it is clear that it did not promote any significant change in the conversion and in the aldol product, resulting in both cases in good levels of *anti/syn* diastereomeric ratio (93:7), excellent conversion (>99%), and a high enantiomeric excess (ee) of 89%, as observed in NMR spectra and chiral-phase HPLC analysis of the *anti* isomer in Figures S5−S7. These measures are better than those for PRW−O-C$_{16}$ under the same conditions (Table 1).[8] On the other hand, considering changes in the water content, we observed that the absence of water hinders the formation of the *anti*-aldol product, producing lower levels of diastereoselectivity (85:15) and enantiomeric excess (68%), with only 62% conversion (Entry 4). These results are similar to those for PRW−O-C$_{16}$ catalyzing the same aldol reaction in the absence of water, with 94% conversion and low diastereoselectivity (86:14), and 73% enantiomeric excess (Table 1).[8] This effect can be associated with the lower level of organization of the lipopeptide molecules, due to the absence of hydrophobic interactions in water that enable self-assembly into micelles. The results are

**Table 1. Results from the Nitro-Aldol Reaction Test of the Reaction between Cyclohexanone and *p*-Nitrobenzaldehyde**

| samples | entry[a] | catalyst (mol %) | cyclohexanone (equiv) | H$_2$O[b] (equiv) | conversion[c] (%) | *anti/syn*[c] | ee[d] (%) |
|---|---|---|---|---|---|---|---|
| PRW−NH-C$_{16}$ | 1[f] | 5 | 12.0 | 2.0 | >99 | 93:7 | 89 |
| | 2 | 5 | 12.0 | 2.0 | >99 | 93:7 | 89 |
| | 3 | 5 | 12.0 | 1.0 | >99 | 93:7 | 88 |
| | 4 | 5 | 15.0 | e | 62 | 85:15 | 68 |
| PRW−O-C$_{16}$ | 5[g] | 5 | 12.0 | 2.0 | >99 | 91:9 | 84 |
| | 6[g] | 5 | 12.0 | 1.0 | >99 | 91:9 | 71 |
| | 7[g] | 5 | 15.0 | e | 94 | 86:14 | 73 |

[a]The reactions were performed at room temperature, for 2 days, with vigorous stirring. [b]Water excess toward cyclohexanone (v/v). [c]The diastereomeric ratios and conversion were determine by ^{1}H NMR analysis of the crude mixture. [d]Determined by chiral-phase HPLC analysis of the *anti* isomer. [e]Neat (no water addition). [f]HFIP was not used. [g]Results presented in ref 8.

interesting since they suggest that changes in the supramolecular state of the lipopeptide molecules influence interactions between the catalyst and the substrate, which could generate steric hindrance of the reagents, and that the presence of water is required to enable these reagents to approach. An additional factor may be the local enhancement of concentration of reagents near the micelle surface in a restricted environment where diastereoselectivity of the reaction could be enhanced.

**Incorporation of PRW-NH-C$_{16}$ into Cubosomes.** As a first step toward the investigation of cubosome particle functionalization with active peptide moieties, we examined the incorporation of PRW-NH-C$_{16}$ into model cubosomes. Although PRW-NH-C$_{16}$ self-assembles in bulk solution, this will be modulated within the lipid channels of a cubosome structure. Lipidation is expected to facilitate insertion of the lipopeptide into the internal bicontinuous membrane within the cubosomes. We first examined the structure of the cubosomes with increasing loading of lipopeptide using a combination of real space imaging (cryo-TEM) and small-angle X-ray scattering (SAXS). The SAXS data is displayed in Figure 3, and the cryo-TEM images are shown in Figures 4 and 5. Control SAXS data for the lipopeptide and F127 solutions are shown in Figure S8, which indicate that F127 is unordered and the lipopeptide forms micelles as evidenced by SAXS form factors similar to those shown in Figure 2b. The SAXS data in Figure 3 contains multiple orders of Bragg reflections due to the bicontinuous cubic structure within the cubosomes. These were indexed as listed in Table 2 and shown in Figure S9. This permitted the determination of the lattice constant for the cubosomes prior to lipopeptide loading, $a = (97.2 \pm 1.2)$ Å. This is within the range of previously reported values (at room temperature) $a = 96.7-97.8$ Å[44,45] (the temperature dependence of $a$ has also been reported[22,46]). There is a significant increase in lattice constant with increasing PRW-NH-C$_{16}$ concentration (Figure 3b), indicating swelling of the aqueous channels within the cubosomes and/or insertion into the lipid bilayer. The SAXS data in Figure 3 shows a progressive loss in the number, and intensity, of reflections upon increased PRW-NH-C$_{16}$ loading. This indicates a loss of long-range cubic order within the cubosomes. This was further examined by cryo-TEM. The images shown in Figure 4 show the high degree of cubic order within cubosomes prior to addition of lipopeptide, along with detailed indexation of reflections obtained from
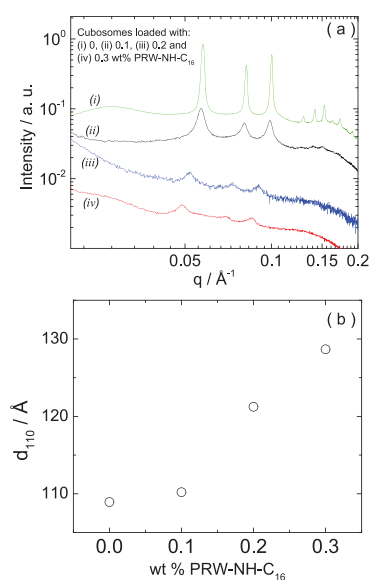


**Figure 3.** (a) SAXS profiles for cubosomes made of 10 wt % monoolein + 1 wt % F127 and loaded with (i) 0, (ii) 0.1, (iii) 0.2, and (iv) 0.3 wt % PRW-NH−CH$_{16}$. (b) Dependence of the spacing of the first reflection in panel a with the concentration of peptide.

Fourier transforms of the images, which in some cases provide monodomain projections of the cubic structure. The indexation is consistent with prior reports on monoolein cubosomes adopting a *Pn3m* cubic structure,[47,48] but with resolution of higher order reflections. Inspection of lower magnification cryo-TEM images such as those shown in Figure 5 indicates a loss of cubosome content upon an increase in lipopeptide concentration, this was quantified by particle counting over multiple images. As shown in the histogram in Figure 5d, the number of cubosomes decreases systematically with an increase in lipopeptide concentration, along with a concomitant increase in the number of vesicles. This indicates that cubosome structure is disrupted by solubilization by PRW-NH-C$_{16}$, leading to the formation of vesicles, which may contain a mixture of monoolein and the lipopeptide or may be monoolein vesicles stabilized by the presence of the lipopeptides in solution. That fact that the lipopeptide was incorporated in the cubosome population was confirmed using a fluorescamine assay of peptide content in the supernatant
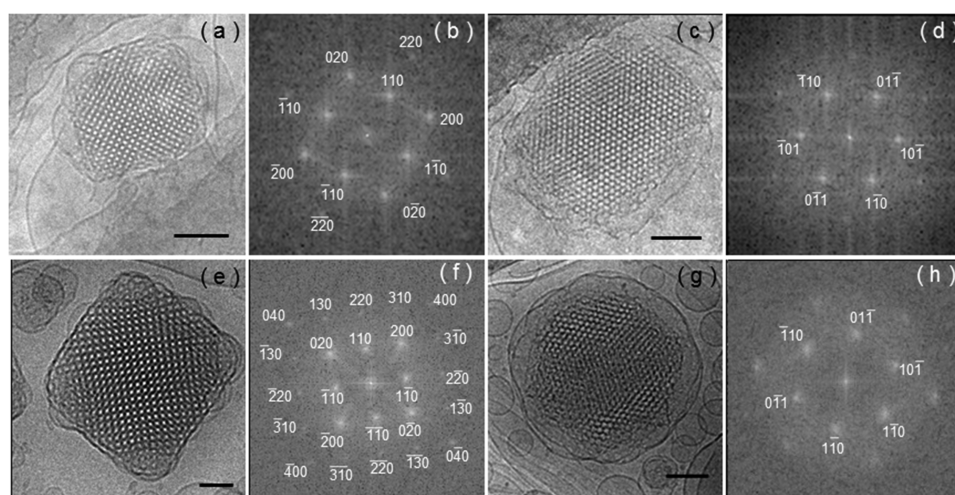
**Figure 4.** Cryo-TEM images of cubosomes made of 10 wt % monoolein + 1 wt % F127 and loaded with (a−d) 0, (e, f) 0.1, and (g, h) 0.3 wt % PRW-NH-$C_{16}$. Scale bars are (a, c, g) 100 or (e) 50 nm. Panels b, d, f, and h are FFT images of panels a, c, e, and g, respectively.
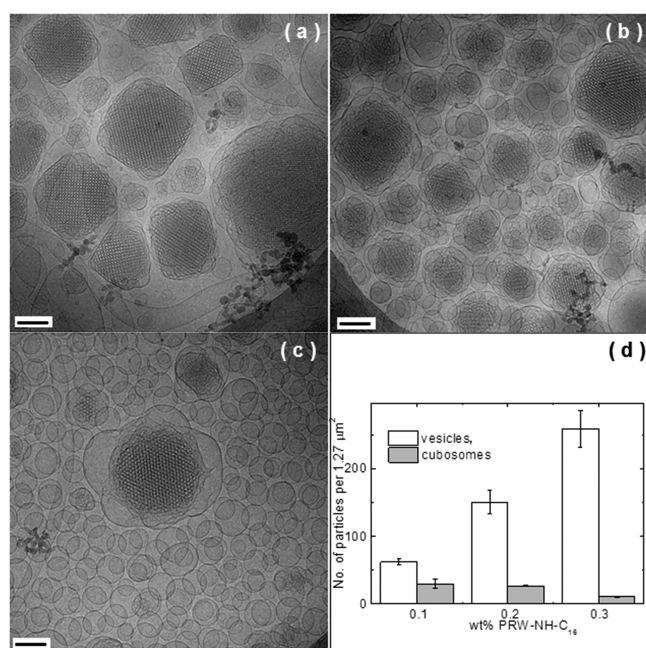


**Figure 5.** Representative cryo-TEM images of cubosomes made of 10 wt % monoolein + 1 wt % F127 and loaded with (a) 0.1, (b) 0.2, and (c) 0.3 wt % PRWNH-$C_{16}$. Scale bars are 100 nm. (d) Counting of cubosomes vs vesicles as a function of the PRW-NH-$C_{16}$ concentration, measured from the corresponding cryo-TEM images.

solution after centrifugation. The spectra in Figure S10 show a progressive increase in fluorescamine fluorescence with increasing PRW-NH-$C_{16}$ concentration, consistent with its release from the cubosomes at a sufficiently high lipopeptide concentration.

**Cytotoxicity of PRW-NH-$C_{16}$.** The cytotoxicity of PRW-NH-$C_{16}$ was examined using model fibroblast and breast cancer (MCF-7) cell lines. The cytotoxicity data is displayed in Figure 6. The assays show that PRW-NH-$C_{16}$ was rather cytotoxic to both cell lines, with a significant loss of viability after 24 h (and more at 72 h) at even the lowest lipopeptide concentration examined (0.005 wt %, which corresponds to 0.05 mg/mL). No significant difference in cytotoxicity was observed with the fibroblasts or breast cancer cells, so PRW-

**Table 2. Summary of Parameters Extracted from the SAXS Data in Figure 3 for Cubosomes Containing 10 wt % Monoolein + 1 wt % F127 and Loaded with 0, 0.1, 0.2, and 0.3 wt % PRW-NH-$C_{16}$**

| PRW-NH-$C_{16}$ (wt %) | spacing (Å) | indexation |
|---|---|---|
| 0 | 108.6 | 110 |
| | 77.0 | 111 |
| | 62.8 | 200 |
| | 48.5 | 211 |
| | 44.3 | |
| | 41.0 | 220 |
| | 38.5 | 221/300 |
| | 36.2 | 310 |
| | 32.8 | 321 |
| 0.1 | 110.9 | |
| | 78.1 | |
| | 63.3 | |
| 0.2 | 121.9 | |
| | 84.8 | |
| | 69.1 | |
| 0.3 | 128.4 | |
| | 89.9 | |
| | 73.2 | |

NH-$C_{16}$ does not display selective anticancer activity under these conditions. These findings extend the previous cytotoxicity assay results for PRW−O-$C_{16}$ (which used a colon cancer cell model), which only extended over a low concentration range (up to 0.005 mg/mL).[29]

## ■ CONCLUSIONS

Through detailed fluorescence and CD/FTIR assays, we show that PRW-NH-$C_{16}$ self-assembles above a critical aggregation concentration, forming structures with PPII peptide conformation. The self-assembled structure above the cac is spherical micelles. This behavior (and the cac value) is very similar to that previously reported for the analogue lipopeptide PRW−O-$C_{16}$ with an ester linker.[8] Thus, the different linker chemistry has very little influence on self-assembly, indicating that it does not greatly influence the amphiphilicity of the molecule. Indeed, it is likely to be "buried" at the interface
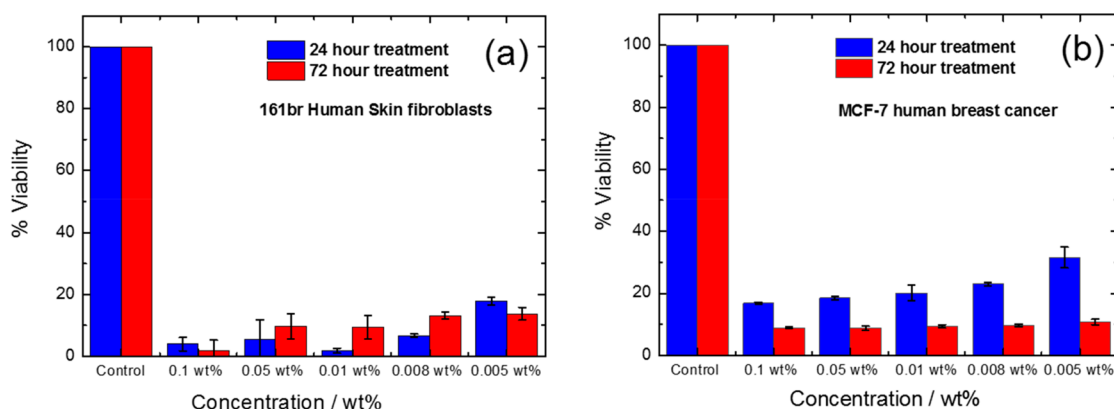
**Figure 6.** Cytotoxicity data, conditions as indicated. Error bars indicate standard deviations of technical errors. (a) 161Br fibroblasts. (b) MCF-7 human breast cancer cells.

between the hydrophobic lipid chain and the hydrated peptide headgroup.

We demonstrated that lipopeptide PRW-NH-$C_{16}$ is able to effectively catalyze a model aldol reaction, with superior conversion and enantiomeric excess compared to PRW–O-$C_{16}$ under comparable reaction conditions.[8] Here, the linker group has an influence potentially due to the differences in the local conformation around the catalytic site and/or the altered polarization of the amide vs ester linkage. The lower micelle radius obtained from SAXS data for PRW–O-$C_{16}$ may reflect a more compact conformation, compared to PRW-NH-$C_{16}$. Relevant to potential bionanotechnological applications, the amide linker should also confer enhanced stability in vivo, due to reduced hydrolysis.

We additionally show for the first time that lipopeptides can be incorporated within cubosomes, using the model monoolein cubosome system, stabilized with the Pluronic block copolymer. A previous report using SAXS to probe the effect of anionic surfactant-like peptides on the lattice spacing of the monoolein *Pn3m* cubic phase (not cubosomes)[45] showed, generally, swelling effects up to defined peptide loadings, at which concentration the cubic order was lost (replaced by hexagonal order). In a study of incorporation of antimicrobial peptides (two neutral and one cationic) into monoolein cubosomes, little change in lattice spacing was observed in the *Pn3m* diamond cubic phase, although significant deswelling was observed for the *Im3m* primitive cubic phase.[26] PRW-NH-$C_{16}$ causes an increase in lattice spacing with an increasing peptide concentration, indicating its incorporation in the cubic phase. It may either swell the water channel or more likely incorporate into the lipid bilayer. Interaction with the lipid bilayer may be enhanced both by favored sequestration of the lipid chain into the lipid membrane (due to the hydrophobic effect) but also interaction between the monoolein glycerol headgroup (hydrogen-bonding capable OH groups) and the peptide. At high loadings, lipopeptide PRW-NH-$C_{16}$ causes a restructuring transition, with a greatly enhanced formation of vesicles (this is accompanied by an increase in the amount of lipopeptide in solution, which may be free lipopeptide and/or lipopeptide self-assembled into micelles). This is a potential strategy to produce vesicles of monoolein, these structures not being observed in the equilibrium phase diagram.[22,49]

Our results show that PRW-NH-$C_{16}$ is rather cytotoxic to both fibroblasts and model cancer cells, presumably due to the strong interaction of the lipopeptide with cell membranes, which incorporate anionic phospholipid headgroups capable to bind arginine residues in the PRW peptide, this being in contrast to the interaction with monoolein, which has a hydrogen-bonding glycerol headgroup. For future applications, it should be possible to modulate the interaction of lipopeptides with different types of lipid membrane by the adjustment of charge and hydrogen-bonding capacity within the peptide sequence and, in this way, to reduce cytotoxicity. Indeed, our group and others are investigating the cytocompatibility of lipopeptides, including examination of selective anticancer activity (which may be achieved by conjugation of small-molecule anticancer molecules).[50−54] This and other promising bioactivities are attractive subjects for further research, and cubosomes are potentially valuable lipopeptide slow release delivery systems. Our initial proof-of-principle work has established that cubosomes can successfully be loaded with a model bioactive lipopeptide.

## ■ ASSOCIATED CONTENT

**Ⓢ Supporting Information**

The Supporting Information is available free of charge on the ACS Publications website at DOI: 10.1021/acsabm.9b00489.

> Additional FTIR spectra, NMR spectra, HPLC chromatogram, fluorescence, SAXS, cytotoxicity and indexation data, and cryo-TEM images (PDF)

## ■ AUTHOR INFORMATION

**Corresponding Author**
*E-mail: I.W.Hamley@reading.ac.uk.

**ORCID** Ⓞ
Valeria Castelletto: 0000-0002-3705-0162
Ian W. Hamley: 0000-0002-4549-0926
Wendel A. Alves: 0000-0002-8394-2751

**Notes**
The authors declare no competing financial interest.

## ■ REFERENCES

(1) Löwik, D. W. P. M.; van Hest, J. C. M. Peptide based amphiphiles. *Chem. Soc. Rev.* **2004**, *33*, 234−245.

(2) Cui, H. G.; Webber, M. J.; Stupp, S. I. Self-Assembly of Peptide Amphiphiles: From Molecules to Nanostructures to Biomaterials. *Biopolymers* **2010**, *94* (1), 1−18.

(3) Matson, J. B.; Zha, R. H.; Stupp, S. I. Peptide self-assembly for crafting functional biological materials. *Curr. Opin. Solid State Mater. Sci.* **2011**, *15*, 225−235.

(4) Hamley, I. W. Self-Assembly of Amphiphilic Peptides. *Soft Matter* **2011**, *7*, 4122−4138.

(5) Dehsorkhi, A.; Castelletto, V.; Hamley, I. W. Self-Assembling Amphiphilic Peptides. *J. Pept. Sci.* **2014**, *20*, 453−467.

(6) Hamley, I. W. Lipopeptides: from self-assembly to bioactivity. *Chem. Commun.* **2015**, *51*, 8574−8583.

(7) Escuder, B.; Rodriguez-Llansola, F.; Miravet, J. F. Supramolecular gels as active media for organic reactions and catalysis. *New J. Chem.* **2010**, *34* (6), 1044−1054.

(8) Soares, B. M.; Aguilar, A. M.; Silva, E. R.; Coutinho-Neto, M. D.; Hamley, I. W.; Reza, M.; Ruokolainen, J.; Alves, W. A. Chiral organocatalysts based on lipopeptide micelles for aldol reactions in water. *Phys. Chem. Chem. Phys.* **2017**, *19* (2), 1181−1189.

(9) Zozulia, O.; Dolan, M. A.; Korendovych, I. V. Catalytic peptide assemblies. *Chem. Soc. Rev.* **2018**, *47* (10), 3621−3639.

(10) Rodriguez-Llansola, F.; Escuder, B.; Miravet, J. F. Switchable Perfomance of an L-Proline-Derived Basic Catalyst Controlled by Supramolecular Gelation. *J. Am. Chem. Soc.* **2009**, *131* (32), 11478−11484.

(11) Rodriguez-Llansola, F.; Miravet, J. F.; Escuder, B. Supramolecular Catalysis with Extended Aggregates and Gels: Inversion of Stereoselectivity Caused by Self-Assembly. *Chem. - Eur. J.* **2010**, *16* (28), 8480−8486.

(12) Rodriguez-Llansola, F.; Escuder, B.; Hamley, I. W.; Hayes, W.; Miravet, J. F. Structural and morphological studies of the dipeptide based L-Pro-L-Val organocatalytic gels and their rheological behaviour. *Soft Matter* **2012**, *8* (34), 8865−8872.

(13) Fu, Y. Q.; An, Y. J.; Liu, W. M.; Li, Z. C.; Zhang, G.; Tao, J. C. Highly diastereo- and enantioselective direct aldol reaction catalyzed by simple amphiphilic proline derivatives. *Catal. Lett.* **2008**, *124* (3−4), 397−404.

(14) Zhong, L.; Gao, Q.; Gao, J. B.; Xiao, J. L.; Li, C. Direct catalytic asymmetric aldol reactions on chiral catalysts assembled in the interface of emulsion droplets. *J. Catal.* **2007**, *250* (2), 360−364.

(15) Yaghmur, A.; Glatter, O. Characterization and potential applications of nanostructured aqueous dispersions. *Adv. Colloid Interface Sci.* **2009**, *147−148*, 333−342.

(16) Chong, J. Y. T.; Mulet, X.; Waddington, L. J.; Boyd, B. J.; Drummond, C. J. Steric stabilisation of self-assembled cubic lyotropic liquid crystalline nanoparticles: high throughput evaluation of triblock polyethylene oxide-polypropylene oxide-polyethylene oxide copolymers. *Soft Matter* **2011**, *7* (10), 4768−4777.

(17) Mulet, X.; Boyd, B. J.; Drummond, C. J. Advances in drug delivery and medical imaging using colloidal lyotropic liquid crystalline dispersions. *J. Colloid Interface Sci.* **2013**, *393*, 1−20.

(18) Murgia, S.; Bonacchi, S.; Falchi, A. M.; Lampis, S.; Lippolis, V.; Meli, V.; Monduzzi, M.; Prodi, L.; Schmidt, J.; Talmon, Y.; Caltagirone, C. Drug-Loaded Fluorescent Cubosomes: Versatile Nanoparticles for Potential Theranostic Applications. *Langmuir* **2013**, *29* (22), 6673−6679.

(19) Hamley, I. W. *Block Copolymers in Solution*; Wiley: Chichester, 2005.

(20) Barauskas, J.; Johnsson, M.; Joabsson, F.; Tiberg, F. Cubic phase nanoparticles (Cubosome): Principles for controlling size, structure and stability. *Langmuir* **2005**, *21*, 2569−2577.

(21) Gustafsson, J.; Ljusberg-Wahren, H.; Almgren, M.; Larsson, K. Cubic lipid-water phase dispersed into submicron particles. *Langmuir* **1996**, *12* (20), 4611−4613.

(22) Qiu, H.; Caffrey, M. The phase diagram of the monoolein/water system: metastability and equilibrium aspects. *Biomaterials* **2000**, *21* (3), 223−234.

(23) Larsson, A.; Dérand, H. Stability of polycarbonate and polystyrene surfaces after hydrophilization with high intensity oxygen RG plasma. *J. Colloid Interface Sci.* **2002**, *246*, 214−221.

(24) Tran, N.; Mulet, X.; Hawley, A. M.; Hinton, T. M.; Mudie, S. T.; Muir, B. W.; Giakoumatos, E. C.; Waddington, L. J.; Kirby, N. M.; Drummond, C. J. Nanostructure and cytotoxicity of self-assembled monoolein-capric acid lyotropic liquid crystalline nanoparticles. *RSC Adv.* **2015**, *5* (34), 26785−26795.

(25) Kluzek, M.; Tyler, A. I. I.; Wang, S. Q.; Chen, R. J.; Marques, C. M.; Thalmann, F.; Seddon, J. M.; Schmutz, M. Influence of a pH-sensitive polymer on the structure of monoolein cubosomes. *Soft Matter* **2017**, *13* (41), 7571−7577.

(26) Meikle, T. G.; Zabara, A.; Waddington, L. J.; Separovic, F.; Drummond, C. J.; Conn, C. E. Incorporation of antimicrobial peptides in nanostructured lipid membrane mimetic bilayer cubosomes. *Colloids Surf., B* **2017**, *152*, 143−151.

(27) Boge, L.; Bysell, H.; Ringstad, L.; Wennman, D.; Umerska, A.; Cassisa, V.; Eriksson, J.; Joly-Guillou, M. L.; Edwards, K.; Andersson, M. Lipid-Based Liquid Crystals As Carriers for Antimicrobial Peptides: Phase Behavior and Antimicrobial Effect. *Langmuir* **2016**, *32* (17), 4217−4228.

(28) Boge, L.; Vastberg, A.; Umerska, A.; Bysell, H.; Eriksson, J.; Edwards, K.; Millqvist-Fureby, A.; Andersson, M. Freeze-dried and re-hydrated liquid crystalline nanoparticles stabilized with disaccharides for drug-delivery of the plectasin derivative AP114 antimicrobial peptide. *J. Colloid Interface Sci.* **2018**, *522*, 126−135.

(29) da Silva, E. R.; Cooney, G.; Hamley, I. W.; Alves, W. A.; Lee, S.; O'Connor, B. F.; Reza, M.; Ruokolainen, J.; Walls, D. Structural Behaviour and Gene Delivery in Complexes Formed Between DNA and Arginine-Containing Peptide Amphiphiles. *Soft Matter* **2016**, *12*, 9158−9169.

(30) Hawe, A.; Sutter, M.; Jiskoot, W. Extrinsic fluorescent dyes as tools for protein characterization. *Pharm. Res.* **2008**, *25*, 1487−1499.

(31) Vivian, J. T.; Callis, P. R. Mechanisms of tryptophan fluorescence shifts in proteins. *Biophys. J.* **2001**, *80* (5), 2093−2109.

(32) Castelletto, V.; Hamley, I. W.; Cenker, C.; Olsson, U.; Adamcik, J.; Mezzenga, R.; Miravet, J. F.; Escuder, B.; Rodriguez-Llansola, F. Influence of End-Capping on the Self-Assembly of Model Amyloid Peptide Fragments. *J. Phys. Chem. B* **2011**, *115*, 2107−2116.

(33) Woody, R. W. Circular Dichroism Spectrum of Peptides in the Poly(Pro)II Conformation. *J. Am. Chem. Soc.* **2009**, *131* (23), 8234−8245.

(34) Woody, R. W. Circular Dichroism. *Methods Enzymol.* **1995**, *246*, 34−71.

(35) Keiderling, T. A.; Xu, Q. *Unfolded Peptides and Proteins Studied with Infrared Absorption and Vibrational Circular Dichroism Spectra*; Academic Press: San Diego, 2002; Vol. 62, pp 111−161.

(36) Pelton, J. T.; McLean, L. R. Spectroscopic methods for analysis of protein secondary structure. *Anal. Biochem.* **2000**, *277*, 167−176.

(37) Gaussier, H.; Morency, H.; Lavoie, M. C.; Subirade, M. Replacement of trifluoroacetic acid with HCl in the hydrophobic purification steps of pediocin PA-1: A structural effect. *Appl. Environ. Microbiol.* **2002**, *68* (10), 4803−4808.

(38) Eker, F.; Griebenow, K.; Schweitzer-Stenner, R. Ab$_{1−28}$ fragment of the amyloid peptide predominantly adopts a polypropy-

line II conformation in acidic solution. *Biochemistry* **2004**, *43*, 6893−6898.

(39) Barth, A. Infrared spectroscopy of proteins. *Biochim. Biophys. Acta, Bioenerg.* **2007**, *1767* (9), 1073−1101.

(40) Barth, A. The infrared absorption of amino acid side chains. *Prog. Biophys. Mol. Biol.* **2000**, *74*, 141−173.

(41) Casal, H. L.; Mantsch, H. H. Polymorphic Phase-Behavior of Phospholipid-Membranes Studied by Infrared-Spectroscopy. *Biochim. Biophys. Acta, Rev. Biomembr.* **1984**, *779* (4), 381−401.

(42) Castelletto, V.; Kirkham, S.; Hamley, I. W.; Kowalczyk, R.; Rabe, M.; Reza, M.; Ruokolainen, J. Self-Assembly of the Toll-Like Receptor Agonist Macrophage-Activating Lipopeptide MALP-2 and of Its Constituent Peptide. *Biomacromolecules* **2016**, *17* (2), 631−640.

(43) Bressler, I.; Kohlbrecher, J.; Thünemann, A. F. SASfit: a tool for small-angle scattering data analysis using a library of analytical expressions. *J. Appl. Crystallogr.* **2015**, *48*, 1587−1598.

(44) Tyler, A. I. I.; Barriga, H. M. G.; Parsons, E. S.; McCarthy, N. L. C.; Ces, O.; Law, R. V.; Seddon, J. M.; Brooks, N. J. Electrostatic swelling of bicontinuous cubic lipid phases. *Soft Matter* **2015**, *11* (16), 3279−3286.

(45) Yaghmur, A.; Laggner, P.; Zhang, S. G.; Rappolt, M. Tuning Curvature and Stability of Monoolein Bilayers by Designer Lipid-Like Peptide Surfactants. *PLoS One* **2007**, *2*, No. e479.

(46) Czeslik, C.; Winter, R.; Rapp, G.; Bartels, K. Temperature-Dependent and Pressure-Dependent Phase-Behavior of Monoacylgly-cerides Monoolein and Monoelaidin. *Biophys. J.* **1995**, *68* (4), 1423−1429.

(47) Yaghmur, A.; de Campo, L.; Sagalowicz, L.; Leser, M. E.; Glatter, O. Emulsified microemulsions and oil-containing liquid crystalline phases. *Langmuir* **2005**, *21* (2), 569−577.

(48) Sagalowicz, L.; Michel, M.; Adrian, M.; Frossard, P.; Rouvet, M.; Watzke, H. J.; Yaghmur, A.; De Campo, L.; Glatter, O.; Leser, M. E. Crystallography of dispersed liquid crystalline phases studded by cryo-transmission on electron microscopy. *J. Microsc.* **2006**, *221*, 110−121.

(49) Kulkarni, C. V.; Wachter, W.; Iglesias-Salto, G.; Engelskirchen, S.; Ahualli, S. Monoolein: a magic lipid? *Phys. Chem. Chem. Phys.* **2011**, *13* (8), 3004−3021.

(50) Hamley, I. W.; Dehsorkhi, A.; Jauregi, P.; Seitsonen, J.; Ruokolainen, J.; Coutte, F.; Chataigné, G.; Jacques, P. Self-assembly of three bacterially-derived bioactive lipopeptides. *Soft Matter* **2013**, *9*, 9572−9578.

(51) Zha, R. H.; Sur, S.; Stupp, S. I. Self-assembly of cytotoxic peptide amphiphiles into supramolecular membranes for cancer therapy. *Adv. Healthcare Mater.* **2013**, *2*, 126−133.

(52) Cheetham, A. G.; Zhang, P. C.; Lin, Y. A.; Lock, L. L.; Cui, H. G. Supramolecular Nanostructures Formed by Anticancer Drug Assembly. *J. Am. Chem. Soc.* **2013**, *135* (8), 2907−2910.

(53) Zhao, H. B.; Yan, L.; Xu, X. G.; Jiang, C. M.; Shi, J. L.; Zhang, Y. W.; Liu, L.; Lei, S. Z.; Shao, D. Y.; Huang, Q. S. Potential of Bacillus subtilis lipopeptides in anti-cancer I: induction of apoptosis and paraptosis and inhibition of autophagy in K562 cells. *AMB Express* **2018**, *8*, 16.

(54) Castelletto, V.; Edwards-Gayle, C. J. C.; Greco, F.; Hamley, I. W.; Seitsonen, J.; Ruokolainen, J., Self-Assembly, Tunable Hydrogel Properties and Selective Anti- Cancer Activity of a Carnosine-Derived Lipidated Peptide *ACS Appl. Mater. Interfaces* **2019**, submitted.